1999

Electrochemical Current Noise on Aluminum Microelectrodes

Joseph W. Isaac
Iowa State University

Kurt R. Hebert
Iowa State University, krhebert@iastate.edu

Journal of The Electrochemical Society, **146** (2) 502-509 (1999)
S0013-4651(98)01-075-1 CCC: $7.00

Electrochemical Current Noise on Aluminum Microelectrodes

Joseph W. Isaac and Kurt R. Hebert*

Department of Chemical Engineering, Iowa State University, Ames, Iowa 50011, USA

Aluminum disk microelectrodes were used to investigate electrochemical current noise in pH 8.8 borate buffer. The current noise spectra, expressed in terms of the current spectral density, had a characteristic two-plateau structure in the experimental bandwidth of 0.05-50 Hz, were potential-independent, and increased proportionally to electrode area. Injection of NaCl solution near the electrode surface, at potentials below that of the onset of pitting corrosion, caused 0.1-1 Hz current fluctuations to appear. From the frequency and area dependence of the current spectral density in the chloride-free solution, it was concluded that the noise arose from a number of discrete, approximately evenly distributed voltage noise sources positioned electrically in series with the inner barrier layer of the oxide film. A mathematical model for the current noise was developed which described a physical mechanism for noise production based on fluctuations in the widths of cracks or pores in the outer part of the surface film. The model was consistent with the observed area and frequency dependence of the current spectral density, suggesting that the physical process it described is a possible mechanism of noise generation. It could not be determined whether the noise sources were isolated defects or flaws, or pores in an outer precipitated portion of the oxide film.

Manuscript submitted January 26, 1998; revised manuscript received September 22, 1998.

Irregular electrochemical current fluctuations on metals with protective oxide films, such as iron, aluminum, and stainless steel, can occur due to stochastic events associated with initiation, growth, or passivation of corrosion pits. In recent years, this electrochemical noise has been extensively studied on a number of metal and alloy systems. On stainless steel, transient bursts of current in chloride solutions have been shown to be caused by the growth and passivation of very small metastable pits at sulfide inclusions.[1,2] In addition, current bursts in chloride-free solutions have been related to the dissolution of sulfide inclusions.[3] The frequency of metastable pitting events is believed to be influenced by the passive current density[1] or surface oxide film thickness,[2] suggesting a possible relationship between pit initiation and film characteristics.

Similar current fluctuations as those on steel can also be found on pure metals, but in the absence of heterogeneities such as inclusions, it has been difficult to ascribe them to features of the film or metal surface. Heusler and co-workers employed spectral analysis to study current noise on iron, both in the presence and absence of chloride ions.[4-6] The addition of chloride ions to the solution produced current fluctuations of magnitude 10-100 pA during the induction period prior to pit formation. With no chloride ions, they showed that the electrochemical noise spectrum was well described by a voltage noise source in series with the oxide film impedance, whose spectral density had a $1/f^2$ dependence on frequency below about 10 Hz. The series relationship of the noise source and film impedance implied that the noise was associated with processes at the metal/film or film/solution interface.

Current bursts on pure aluminum have been found in chloride solutions at potentials within a range 100-200 mV cathodic of the pitting potential.[7-9] Typical current bursts were tens of nanoamperes in magnitude and 0.1-1 s duration. Pride et al.,[9] through microscopic observations, showed that these current bursts were due to growth and repassivation of metastable pits. Uruchurtu and Dawson investigated open-circuit potential noise on pure aluminum during pitting in chloride solution.[10] They suggested that pit initiation occurred by the sudden activation of metal by chloride ions at pre-existing flaws or defects in the oxide film, at the base of which metal may be intermittently exposed, for example, by mechanical cracking in response to stress in the film. Similar views on the importance of flaws as pitting sites have also been advanced by other authors.[11-13] Recently, electron optical evidence for flaws in aluminum oxide films has been provided by Thompson, Shimizu, and co-workers.[14,15]

The present work concerns the relationship between the electrochemical current noise on aluminum and the structure of the surface oxide film. If the film contains flaws or defects as suggested previously, these flaws may function as local current sources, even in the absence of conditions that lead to pitting corrosion. Current noise may be generated, for example, by intermittent oxide breakdown and repassivation of these sites. Thus, analysis of the current noise in chloride-free solutions may provide information relevant to the presence of flaws in the oxide film. Another noise source may be related to porosity in the outer part of the oxide film, as current noise has previously been associated with the roughness of zinc electrodeposits.[16]

The electrodes used in this work were disk microelectrodes with diameters from 25 to 508 μm, and most of the measurements were carried out in pH 8.8 borate buffer solution. The use of microelectrodes allowed the dependence of the current noise on the electrode area to be obtained, which is relevant to the spatial distribution of noise sources. Additionally, some measurements of current noise after addition of NaCl to the buffer solution are reported. However, the current bursts associated with metastable pitting in chloride solutions were not the main focus of this investigation.

The current noise in the chloride-free solution was quantified through the current spectral density, S_I (referred to frequently as the current power spectral density), defined by

$$S_I = \frac{2}{t_m}\left|I(f)\right|^2 \qquad [1]$$

where t_m is the measurement period and $I(f)$ is the component of the Fourier transform of the current at frequency f. S_I represents the contribution of a differential range of frequency to the variance of the current signal. A mathematical model to predict the frequency and area dependence of S_I was developed to interpret the noise measurements in terms of a physical mechanism. The model was based on noise models used for biological membranes and semiconductor devices,[17,18] and incorporated structure-dependent electrical characteristics of the oxide film. Similar modeling procedures have been applied previously in other investigations of electrochemical noise.[19-22]

Experimental

Electrodes were fabricated from 99.99% purity Al wires of various diameters [25, 50, and 125 μm (Goodfellow); 254 and 508 μm (ESPI)]. Wires were coated with epoxy, which was allowed to dry, and then the wires were fixed with additional epoxy inside glass capillaries so that the tips of the wires protruded from the capillaries. The wires were severed at the protruding ends. Microscopic observation indicated that the resulting electrodes were disk-shaped and that no crevices were present. The reference electrode was a saturated calomel electrode (SCE) and the counter electrode was a platinum wire. The volume of the cell solution was 50 mL. The cell solution

* Electrochemical Society Active Member.

S0013-4651(98)01-075-1 CCC: $7.00

composition was 0.1 M boric acid and 0.5 M sodium borate and its pH was 8.80.

Polarization was applied with a low-noise potentiostat, which was based on the design of Howell and co-workers,[23] and built in house. The current follower gain was 15.1 mV/nA. The potentiostat was powered by a battery to minimize noise, and both it and the cell were placed in a Faraday cage. Constant potential inputs were supplied to the potentiostat using a battery equipped with a voltage divider, which was also placed within the Faraday cage. Current output from the experiments was recorded by a high-speed digital voltmeter located outside the Faraday cage (Keithley 194A) whose resolution was 10 μV.

In all experiments, the cell current was allowed to reach steady state before measurements were started. Steady state was approached in typically 5-10 min. Noise spectra were derived from current time series measured at constant potential. In each time series, the current was sampled at intervals of 10 ms for a period of 40 s. After one 40 s time series was measured in the borate buffer, 1 mL of 1.0 M NaCl solution was injected into the cell near the electrode surface. This injected solution was unbuffered and its pH was 6.1. Two additional 40 s time series were then measured: one immediately after injection and another 120-160 s after injection. Further experimental details are available elsewhere.[24]

Current spectral densities over the frequency range 0.05-50 Hz were calculated from the time series measurements in borate buffer, using statistical software (IMSL subroutine SSWD). This spectral analysis used the Parzen spectral window with a window parameter M of 500. The 90% confidence interval of the calculated spectrum was from 0.684 S_I to 1.63 S_I, and the 80% confidence interval was from 0.745 S_I to 1.46 S_I, where S_I is the local spectral density at a given frequency.

Results

The sensitivity of the measurement system was determined in experiments where constant potentials were applied across resistors whose resistances ranged from 1 to 15 mΩ. Figure 1 shows S_I for a 15 mΩ resistor at three different applied potentials. Above 1 Hz the spectral density was independent of current and frequency. This high-frequency noise decreased slightly with increasing resistance but remained at about 1×10^{-25} A^2/Hz, equivalent to a root-mean-square (rms) noise current of 2 pA in the frequency band 1-50 Hz. In electrochemical experiments, the smallest value of S_I above 1 Hz was 1×10^{-24} A^2/Hz, an order of magnitude larger than the resistor noise. Below 1 Hz, S_I was approximately proportional to $1/f$ and increased with current. Generally, $1/f$ noise is associated with energy dissipation during the flow of current, and its magnitude is proportional to I^2R, where I is the current and R is the resistance of the conductor.[17] S_I in the low-frequency region increased with both current and resistance, in agreement with this expectation.

In electrochemical experiments, current time series were acquired at a number of constant potentials in the passive range: −1.0, −0.95, −0.90, −0.85, −0.80, and −0.7 V. The mean currents in each time series are shown in Fig. 2. While scattered, there is a clear increase of the currents with electrode area; no potential dependence is evident. The line passing through the data was determined by linear regression and has the equation $I = 1.85 \times 10^{-7} A^{0.520}$, with I in amperes and A in cm^2. Figure 3 shows the current spectra from experiments with the electrodes of various diameters at the same potential of −0.7 V in borate buffer. The spectra could be represented by a two-plateau structure, with a low-frequency plateau below about 0.1 Hz followed at higher frequencies by a decay of S_I and then a high-frequency plateau. In the following, the maximum frequency of the low-frequency plateau is referred to as the low breakpoint frequency and the minimum frequency on the high-frequency plateau as the high breakpoint frequency. Figure 3 also demonstrates that the spectra generally increased uniformly with electrode area. Given the statistical confidence intervals described for the spectral density, all features of the spectrum were quantitatively certain except the low breakpoint frequency. However, since nearly all spectra displayed a low-frequency plateau, it is taken to be a valid feature of the spectra.

An example of a current time series measured upon injection of NaCl solution is shown in Fig. 4. After injection, the current rose to a peak and then decayed. In all the experiments, the average ratio of the peak current to initial current was 1.4 and the decay time ranged from 5 to 30 s. During these decays, low-frequency current fluctuations were sometimes present, such as the one between 10 and 20 s in Fig. 4. Such fluctuations were found only in the spectra from time series 0-40 s after NaCl injection and not in those before injection nor 120-160 s after injection. In addition, injection of borate buffer instead of NaCl produced no effect on the current noise spectra.[24] The presence of the current decays was found to introduce significant error into the calculation of the noise spectra just after NaCl injection, since the requirement for a stationary time series was violated. For this reason, only current noise spectra in borate buffer alone are presented here.

The spectral measurements in borate buffer can be summarized in terms of their characteristic breakpoint frequencies and current

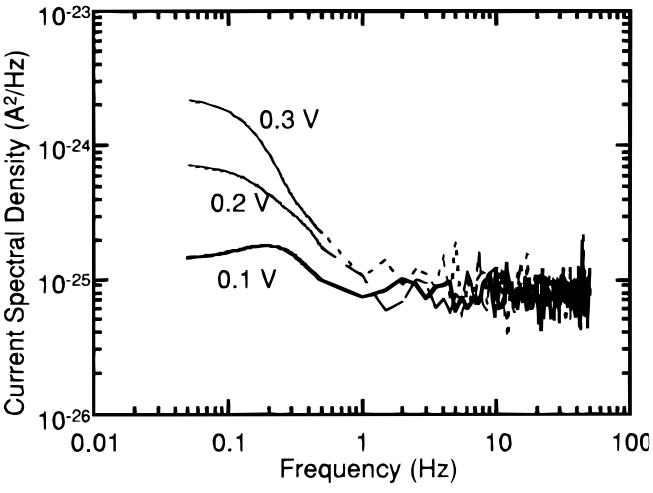

Figure 1. Current spectral density of 15 MΩ resistor at various applied potentials.

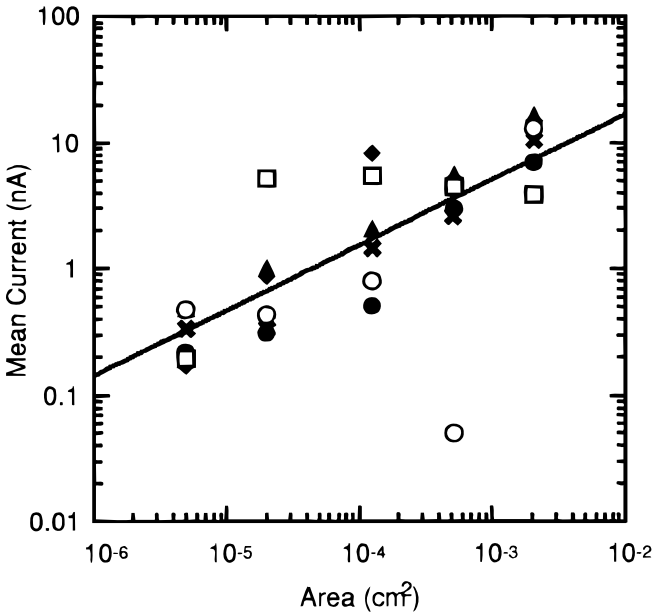

Figure 2. Mean current over 40 s at constant potentials between −1.0 and −0.7 V as a function of the microelectrode area. (——) Is a linear regression fit. Symbols are various applied potentials vs. SCE: (●) −1.0, (×) −0.95, (○) −0.90, (□) −0.85, (◆) −0.80, and (▲) −0.70 V.

S0013-4651(98)01-075-1 CCC: $7.00

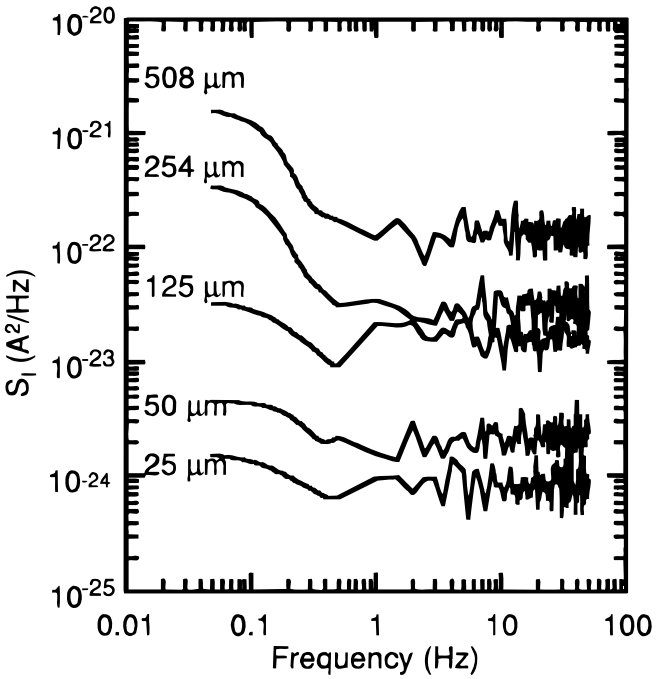

Figure 3. Current spectral density of six disk microelectrodes at −0.7 V. Electrode diameters are indicated.

noise plateaus. The low and high breakpoint frequencies (Fig. 5) were taken as the end points of the linear portion of the decay at intermediate frequencies. The breakpoint frequencies did not depend on the potential, and as the figure shows, there was also no dependence on the electrode area. The mean low and high breakpoint frequencies were 0.14 ± 0.025 and 0.31 ± 0.060 Hz (95% confidence intervals), respectively. The negative slope of the decay of S_I in intermediate frequencies, when S_I plotted on logarithmic axes, is shown in Fig. 6 as a function of electrode area. The decay slope is calculated by dividing the ratio of the height of the low-frequency plateau to

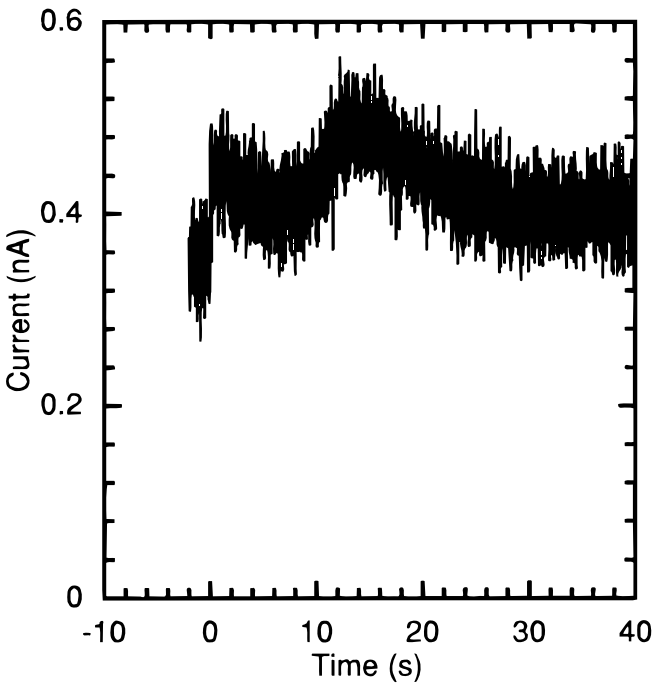

Figure 4. Current transient on 25 μm diam microelectrode at −0.95 V after NaCl injection (at zero time).

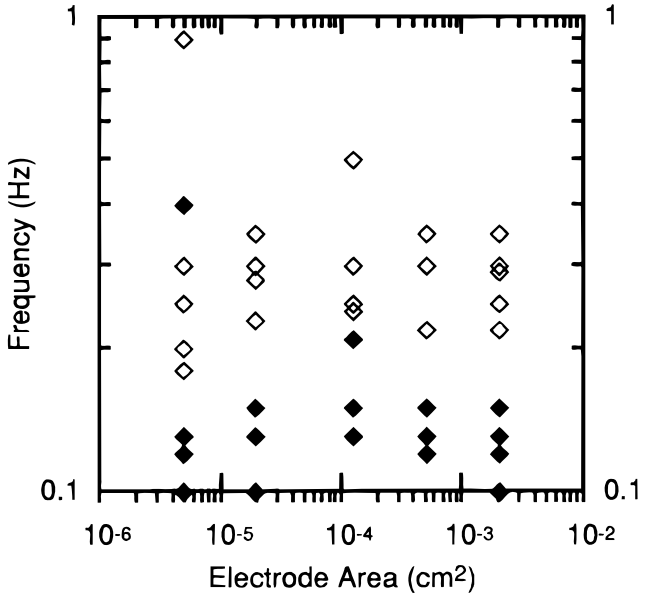

Figure 5. Low and high breakpoint frequencies vs. electrode area. Open markers represent high breakpoint frequencies and solid markers low breakpoint frequencies. Multiple data points at each area are for different applied potentials.

that of the high frequency plateau by the ratio of the high breakpoint frequency to the low breakpoint frequency. While the decay slopes were widely scattered, there was apparently no potential or area dependence. The mean decay slope was 2.06 ± 0.53 (95% confidence interval), suggesting a roughly $1/f^2$ dependence of S_I in the decaying region at intermediate frequencies.

The dependence of S_I in the high frequency plateau on electrode area is shown explicitly in Fig. 7. The figure indicates a direct proportionality between the spectral density and electrode area, according to the relation $S_I = (1 \times 10^{-19}\ A^2/Hz\ cm^2)\ A$, where A is the electrode area. The corresponding (rms) noise current density is

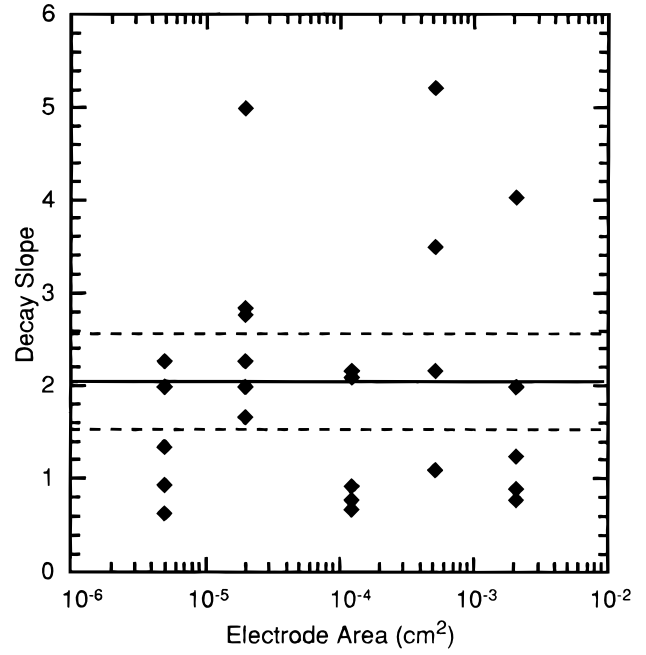

Figure 6. Decay slopes of log S_I vs. log f plotted against electrode area: (——) average decay slope 2.06 and (– – –) represents 95% confidence intervals drawn with a slope of two. Multiple data points at a given area represent different applied potentials.

S0013-4651(98)01-075-1 CCC: $7.00

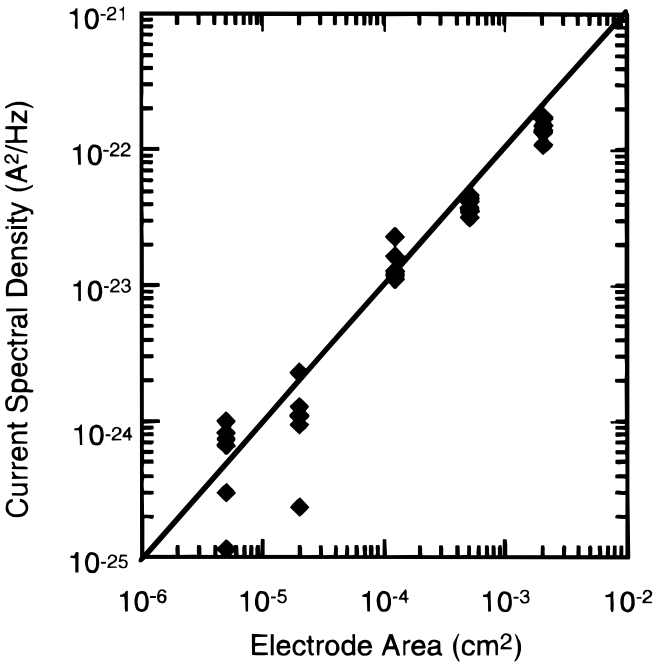

Figure 7. Average current spectral density, S_I, between 5 and 50 Hz as a function of electrode area. Multiple data points at a given area represent different applied potential. (——) Represents a direct proportionality between spectral density and area.

(2 pA/cm) $A^{-1/2}$. The close adherence of the data to this relationship confirms that the noise was electrochemical in origin, since noise from instrumental or external sources would not be expected to depend on electrode area.

Mathematical Model

In this section a physical model for the current noise measurement is given. Conclusions are drawn about the nature of the electrochemical noise sources based on the comparison of this model with the experimental spectra.

Contribution of thermal conduction noise.—Thermal conduction noise, i.e., noise due to the random thermal motion of current-carrying ions, is given by

$$S_I^{th} = 4kT\,Re\left(\frac{1}{Z}\right) \qquad [2]$$

where $Re(1/Z)$ is the real part of the reciprocal of the electrode impedance.[17] For aluminum at potentials in the passive region, the impedance is assumed to be dominated by the resistance and capacitance of the surface oxide film, and $Re(1/Z)$ is approximately g_2A, where g_2 is the conductance of the film. Hence, the thermal current noise is frequency-independent and increases linearly with electrode area. It can be estimated using a value of g_2 of 1.2×10^{-5} A/V cm^2, which was obtained from the current transient measurements of Wilhelmsen and Hurlen on aluminum electrodes in solutions of neutral pH.[25] Equation 3 then becomes $S_I^{th} = (2.0 \times 10^{-25}$ A^2/cm^2 Hz$)A$. By comparison to Fig. 7, this theoretical thermal conduction noise is 5×10^5 times smaller than the experimental current noise in the high-frequency plateau. Also, it does not have the observed two-plateau dependence on frequency. This suggests that the experimental noise should be explained by some other process.

Analysis of the mean current measurements.—The mean current measurements in Fig. 2 can provide information about the metal dissolution process, which is relevant in the formulation of the noise model. The dependence of the current on $A^{0.52}$ suggests possible diffusion control of dissolution. The diffusion flux of dissolved aluminum at steady state away from a disk microelectrode is

$$N_{Al} = \frac{D_{Al}C_{Al}}{a} \qquad [3]$$

D_{Al} and C_{Al} are the diffusivity and surface concentration of aluminate [$Al(OH)_4^-$] ions, the predominant dissolved aluminum species at pH 8.8. This expression yields for the current $I = 3\pi^{1/2}FD_{Al}C_{Al}A^{1/2}$. The exponent 1/2 on the area is close to that in Fig. 2. From the intercept of Fig. 2 and using a value of 1.3×10^{-5} cm^2/s for D_{Al},[26] C_{Al} is found to be 2.8×10^{-5} M. The current independence of C_{Al}, as suggested by the results, would be expected if the solution near the oxide surface were in equilibrium with the film. The solubility equilibrium constant implied by the data is C_{Al}/C_{OH^-}, or 4.4. This value is close to the solubility product of pseudoboehmite, a hydrated aluminum hydroxide, which is 6.3.[27] Since the surface layers of the film probably contain appreciable quantities of hydroxide ions and water, it is reasonable to expect that its solubility constant would be similar to that of this material. Therefore, the mean current data are consistent with diffusion-controlled steady-state dissolution and equilibrium of the film surface with the adjacent solution. More extensive experiments would be necessary to confirm this hypothesis. However, Heusler and Allgaier showed through aluminum rotating disk electrode experiments in solutions of pH greater than 11, that the solution at the electrode surface was saturated with aluminum, and dissolution was controlled by mass transfer.[26] The present results are consistent with theirs but apply to a lower pH of 8.8. Kaesche concluded that the aluminum dissolution rate in Na_2SO_4 solution was diffusion-controlled between pH 7 and 10, although data under controlled hydrodynamic conditions were not reported.[28]

Formulation of the noise model.—If the film surface is in equilibrium with the adjacent solution, the outer portion of the film may have a porous structure consisting of precipitated solid particles. This implies that the film should be viewed as composed of an inner compact barrier layer and an outer porous layer. If the film does not have such a precipitated outer layer but contains flaws or defects, forming easy conduction paths, flaw conduction can be considered as electrically in series with conduction in the barrier layer. The duplex porous layer/barrier-layer model can also be used to describe this situation. Hence, the duplex model of the oxide film used here is understood to represent either a film with a precipitated outer portion or one with flaws. It is proposed that fluctuations in the widths of the pores (or flaws) in the porous layer generate the observed current noise. If the pore solution is saturated with aluminum ions, fluctuations in the pore concentration would be significant due to the very small pore dimensions and would cause the pore solution to alternate between undersaturated and supersaturated conditions. In response, the pore diameters would fluctuate as oxide dissolved from and deposited on the pore walls. An alternative mechanism for pore width fluctuations could be the intermittent cracking and repassivation of mechanical flaws located in regions of stress concentration.[10] In the model, the pore fluctuations are viewed in simple terms by a two-state channel concept in which a pore alternates between "open" and "closed" conditions, as depicted in Fig. 8a and b. As individual pores open and close, the number of open pores in the film fluctuates. Similar models have been used to describe noise associated with biological membranes.[17]

According to the two-state channel model, the number of pores in the open state, N_o, is determined by a kinetic balance equation describing the process of pore opening and closing

$$\frac{dN_o}{dt} = k_1(N_t - N_o) - k_2N_o + H(t) \qquad [4]$$

On the right side of the equation, the first term represents the conversion of closed pores to open pores (by dissolution or cracking, for example) and the second conversion of open to closed pores (by precipitation or repassivation). Fluctuations of N_o are described by the random variable $H(t)$. This method of modeling noise through the use of balance equations with random generation terms is known as

S0013-4651(98)01-075-1 CCC: $7.00

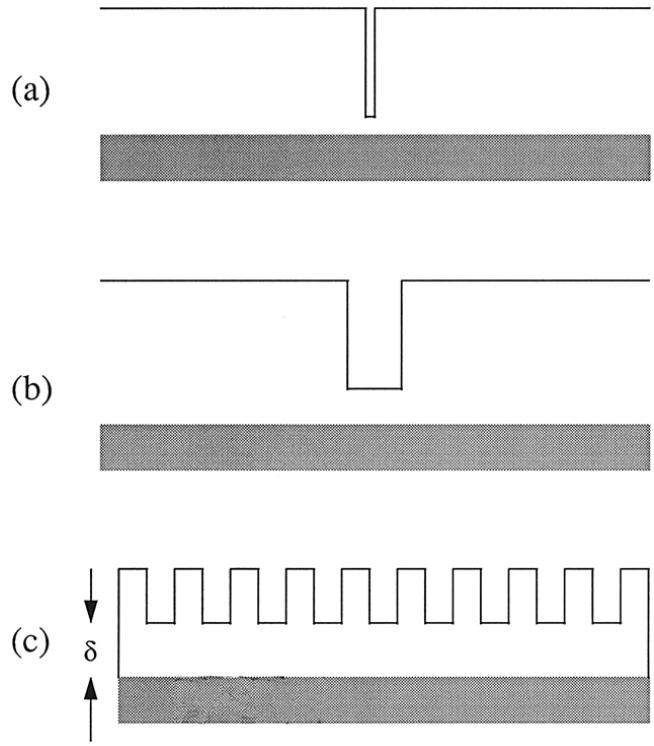

Figure 8. Schematic drawings of models of the surface film: (a) pore in "closed" state, (b) pore in "open" state, and (c) representation of the film as a two-layer structure with an inner barrier layer of thickness δ and outer porous layer.

the Langevin approach.[18] Because $H(t)$ is assumed to be composed of mutually independent random events, its spectral density $S_H(f)$ is frequency-independent; that is, $H(t)$ is "white noise." Equation 4 is linearized about the steady-state condition to obtain

$$\frac{dN'_o}{dt} = -\frac{1}{\tau}N'_o + H(t) \quad [5]$$

where τ is $(k_1 + k_2)^{-1}$. Primed variables in the model are deviations from steady state during fluctuations.

The variation with time of the number of open pores produces fluctuations of the electrical characteristics of the film. A schematic view of the two-layer film model, depicting the inner, solid-conducting barrier layer (thickness δ), and the outer, aqueous-conducting porous layer is shown in Fig. 8c. The porous layer conductance is likely to be large and is not included in the model. However, electrochemical measurements on aluminum and other metals indicate that the electrochemical overpotential due to ion transfer processes at the oxide/solution interface can be significant.[29,30] Thus, the electrical model of the film includes both barrier-layer conduction resistance and the interfacial kinetic resistance of ion-transfer reactions.

The additional model equations needed to describe electrochemical processes are the expressions for current at the film/solution interface and through the barrier layer, and the potential balance equation. The current at the interface is

$$I = N_o A_p\left(C_p\frac{d\phi_3}{dt} + i_{co}e^{b_c\phi_3}\right) \quad [6]$$

which is linearized to obtain

$$I' = \overline{N}_o A_p\left(C_p\frac{d\phi'_3}{dt} + g_p\phi'_3\right) + I_p N'_o \quad [7]$$

Here, g_p is the kinetic interfacial conductance, $b_3 i_{co}\exp(\overline{b_3\phi}_3)$, and I_p is the current passing through one pore, $i_{co}A_p\exp(b_3\overline{\phi}_3)$. In this equation and the following ones, barred variables represent values in the steady state. The current in the barrier layer obeys

$$I = C_2 A\frac{d\phi_2}{dt} + i_{ao}\exp\left(\frac{B\phi_2}{\delta}\right)A \quad [8]$$

in which the two terms on the right side are the capacitive and conduction contributions to the current through the barrier layer. The latter is taken to obey high-field conduction kinetics.[31] In linearized form this equation is

$$I' = C_2 A\frac{d\phi'_2}{dt} + g_2 A\phi'_2 \quad [9]$$

where g_2 is the conductance of the barrier layer, $i_{ao}B/\delta\exp(B\overline{\phi}_2/\delta)$. The final equation states that since the applied potential is constant, ϕ_3 and ϕ_2 add together to a constant value

$$E = \phi_2 + \phi_3 + \phi^* \quad [10]$$

where ϕ^* represents the sum of all constant potential drops in the system, including the reference electrode and the metal/barrier layer interface. In terms of deviation variables, this equation is

$$0 = \phi'_2 + \phi'_3 \quad [11]$$

Equations 5, 7, 9, and 11 constitute the model. The solution for the current spectral density follows the procedure given by van der Ziel.[18] The dependent variables are represented in terms of Fourier components, for example

$$I' = \sum_{k=-\infty}^{\infty} I'_k e^{j\omega_k t} \quad [12]$$

Omitting the k subscripts, the equations for the Fourier coefficients corresponding to Eq. 5, 7, and 9 are

$$j\omega N'_o = H - \frac{1}{\tau}N'_o \quad [13]$$

$$I' = \overline{N}_o A_p(j\omega C_p\phi'_3 + g_p\phi'_3) + I_p N'_o \quad [14]$$

$$I' = j\omega C_2 A\phi'_2 + g_2 A\phi'_2 \quad [15]$$

while the form of Eq. 11 is unchanged when written in terms of Fourier coefficients. The equations were solved to obtain the current fluctuation amplitude $I'(\omega)$ in terms of the random variable $H(\omega)$, yielding

$$\frac{I'(\omega)}{H(\omega)} = \left(\frac{I_p\tau g_2}{g_2 + g_3}\right)\frac{1 + j\dfrac{\omega}{\omega_2}}{\left(1 + j\dfrac{\omega}{\omega_1}\right)\left(1 + j\dfrac{\omega}{\omega_3}\right)} \quad [16]$$

in which g_3 is ϵg_p, where the porosity ϵ is $\overline{N}_o A_p/A$. The characteristic frequencies ω_1, ω_2, and ω_3 are $(g_2 + \epsilon g_p)/(C_2 + \epsilon C_p)$, g_2/C_2, and $1/\tau$, respectively. The relation between this expression and the spectral density $S_I(\omega)$ is

$$\frac{S_I(\omega)}{S_H(0)} = \left(\frac{I'}{H}\right)\left(\frac{I'}{H}\right)^* \quad [17]$$

where the asterisk indicates the complex conjugate. The expression $S_H(0)$is used because S_H is a constant since it is frequency independent. The result is

$$\frac{S_I(\omega)}{S_H(0)} = \left(\frac{I_p\tau g_2}{g_2 + g_3}\right)^2\frac{1 + \left(\dfrac{\omega}{\omega_2}\right)^2}{\left(1 + \left(\dfrac{\omega}{\omega_1}\right)^2\right)\left(1 + \left(\dfrac{\omega}{\omega_3}\right)^2\right)} \quad [18]$$

Equation 18 contains the constant $S_H(0)$, which can be related to the variance of the porosity[18]

$$S_H(0) = \frac{4}{\tau}\sigma_N^2 \quad [19]$$

S0013-4651(98)01-075-1 CCC: $7.00

In the two-state channel model, the pore statistics are governed by a binomial distribution, according to which the variance of N_o is $p(1-p)n_tA$. [17] Here, p is the probability that a channel is open. Accordingly, $S_H(0)$ is

$$S_H(0) = \frac{4}{\tau} n_t p(1-p)A \qquad [20]$$

p is found to be $k_1/(k_1 + k_2)$ by solving Eq. 4 for the steady-state porosity. $S_H(0)$ thus depends on parameters whose values cannot be determined from electrochemical measurements alone. For this reason, a direct numerical comparison between the predicted and experimental current spectral densities cannot be carried out. However, as described in the following section, predictions of the model about the shape and area dependence of the spectra can be compared directly with experiment.

Discussion

In this section, the theoretical spectra and experimental results are discussed with regard to their area dependence and frequency dependence. Then the model is used to relate the current noise to the flaw number density.

Dependence of S_I *on area*.—According to Fig. 6, the predicted current spectral density from Eq. 18 should be proportional to electrode area at all frequencies. In that equation both g_2 and g_3 are proportional to the mean current density, which in turn is proportional to $A^{-1/2}$ (Fig. 2). Since the area dependences of the conductances cancel, the area dependence of S_I is determined by that of $S_H(0)$, which from Eq. 20 is seen to be proportional to A. Thus, the model gives the correct dependence of the spectral density on electrode area.

Dependence of S_I *on frequency*.—The shape of the spectrum is determined by the values of the characteristic frequencies ω_1, ω_2, and ω_3. ω_2, the frequency of the resistive-capacitive relaxation of the inner layer, is found in ac impedance spectra and other electrochemical transient measurements. For example, according to Wilhelmsen and Hurlen,[25] g_2 is 1.2×10^{-5} A/V cm^2 and C_2 is 9.8 μF/cm^2, from which ω_2 is 1.2 s^{-1} or f_2 (i.e., $\omega_2/2\pi$) is 0.19 Hz. Krishnakumar and Szklarska-Smialowska report that f_2 was 0.41 Hz upon immersion in 0.3 wt % NaCl below the pitting potential and increased to 0.48 Hz after about 1 h.[13] Two other studies report comparable values. Bessone et al.[32] give g_2 as 2.0×10^{-5} A/V cm^2 and C_2 as 8.0 μF cm^2 at pH 6, from which f_2 is 0.40 Hz, and the impedance spectra of Lenderink et al.[33] indicate that f_2 is several tenths of a hertz. From Fig. 4, the high breakpoint frequency (0.31 Hz) was closest to these values and therefore this frequency is assigned to f_2. It is also noted that the predicted overall shape of the spectrum depends on the order of f_1, f_2, and f_3. If f_2 is intermediate between f_1 and f_3, the spectrum has two plateaus, the one at low frequencies higher than that at high frequencies, and f_2 is the minimum frequency of the high-frequency plateau. This shape is consistent with the experimental spectra. The spectrum would have no plateaus if f_2 were greater than f_1 and f_3; if f_2 were less than f_1 and f_3, the height of the low frequency plateau would be less than that of the high frequency plateau. Therefore, the assignment of f_2 to the high breakpoint frequency is consistent with impedance measurements and is the only one which produces the correct shape of the experimental spectra.

Given the assignment of f_2 to the high breakpoint frequency, the low breakpoint frequency of 0.14 Hz can be either f_1 or f_3. The choice of either f_1 or f_3 as the low breakpoint frequency does not influence the shape of the spectrum predicted by Eq. 18. Ellipsometric measurements reported by Krishnakumar and Szklarska-Smialowska indicated the appearance of a distinct outer layer in the surface film, in experiments for which a second resistive-capacitive relaxation (in addition to that of the barrier layer) was found in impedance spectra at frequencies around 0.1 Hz. This result suggests that the low breakpoint frequency might be taken as f_1, the resistive-capacitive characteristic frequency of the outer porous layer. However, this assignment must be considered tentative, since impedance spectra on aluminum do not always indicate the presence of such a low-frequency RC relaxation. Whether f_1 or f_3 is taken as the low breakpoint frequency, the remaining one should then be greater than f_2. According to Eq. 18, this characteristic frequency would appear as an upper limit on the high frequency plateau, above which S_I would decrease proportionally to f^2. Since no such upper limit is found in the experimental spectra, this frequency must be greater than the upper limit of the experimental bandwidth, 50 Hz.

The theoretical noise spectrum is shown in Fig. 9, where S_I was normalized by dividing by the high frequency plateau. f_1 is taken as 0.14 Hz, f_2 as 0.31 Hz, and f_3 is assumed to be higher than 50 Hz. The spectrum shows the same two-plateau structure found in the experimental spectra in Fig. 3. The spectral density plateau ratio in the figure is 1.9 times larger than the breakpoint frequency ratio, close to the mean decay slope of 2.06 found from Fig. 6 and well within the error bars of the decay slope. Thus the shape of the experimental spectra is modeled reasonably by the ω dependent factor in Eq. 18.

The relationship of the shape of the spectrum and the physical noise mechanism described by the model can be understood with reference to the porous layer current equation, Eq. 15. The fluctuations in N_o cause the area of the oxide/solution interface to fluctuate. According to Eq. 15, the variations of interfacial area can be thought of as producing either fluctuations of current at constant ϕ_2, fluctuations of ϕ_2 at constant current, or a combination of these. If the former process of direct current fluctuations were dominant, S_I would have been given by

$$\frac{S_I(\omega)}{S_H(\omega)} = (I_p\tau)^2 \frac{1}{1 + \left(\frac{\omega}{\omega_1}\right)^2} \qquad [21]$$

This equation is derived by setting ϕ'_2 to zero in Eq. 15. Thus, the spectrum would not have the high frequency plateau as observed experimentally. The appearance of a high frequency plateau, with a high breakpoint frequency identifiable as the characteristic RC frequency of the barrier oxide layer, is evidence that the ϕ_2 fluctuation mechanism at least makes a significant contribution to the current noise. A general way of characterizing the measured current noise which does not depend on the physical model presented here is that it derives from a voltage noise source in series with the impedance of the barrier layer. Interestingly, the same conclusion was reached by Nachstedt and Heusler in the analysis of their current noise meas-

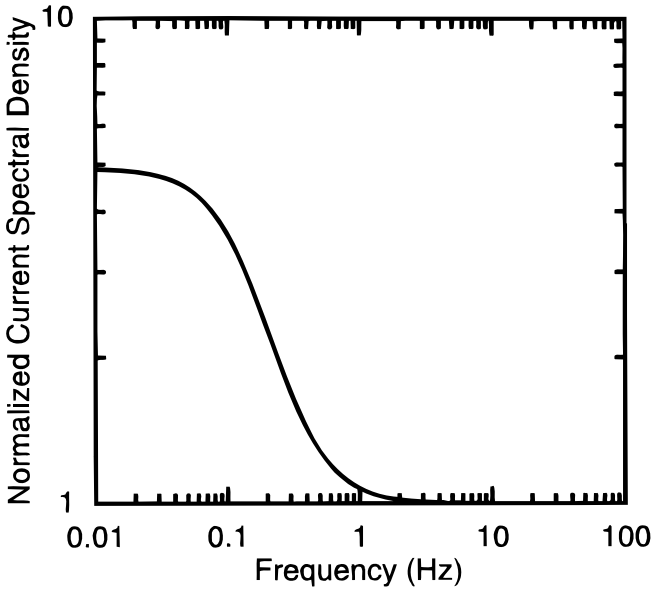

Figure 9. Theoretical current noise spectrum in which S_I has been normalized by dividing by the high-frequency plateau. f_1 taken as 0.14 Hz and f_2 as 0.31 Hz.

S0013-4651(98)01-075-1 CCC: $7.00

urements on iron.[4,5] Thus, common mechanisms may contribute to electrochemical noise on both metals.

The noise measurements support the porous layer/barrier model of the film and the mechanism of pore width fluctuations. If one accepts that the noise arises from small-scale localized processes, the proportionality of S_I to area indicates that these noise sources are distributed approximately evenly across the metal surface. However, the physical significance of the noise sources, whether they represent flaws or aqueous paths through a precipitated layer, cannot be determined from the noise measurements alone. For this purpose, impedance measurements coupled with high-resolution microscopic images would be useful.

Response to injection of NaCl solution.—The model also gives a possible explanation for the low-frequency noise features found in the current time series measured immediately after injection of NaCl solution near the electrode (Fig. 4). These current noise features are not similar in shape to current bursts associated with metastable pitting on aluminum in chloride solutions.[8,9] Their time scale indicates that they are associated with frequencies around the range 0.1 Hz, in the region of the low frequency plateau. According to Eq. 18, S_I in this plateau is given by the frequency-independent factor, which is proportional to the pore current I_p squared. Since I_p is proportional to the pore cross-sectional area, enlargement of pores by dissolution of oxide on their walls would be one process by which the low-frequency noise would be enhanced. In fact, upon injection the pH near the oxide surface would have decreased abruptly from the buffer pH of 8.8 to a value at least as acidic as the injected solution pH 6, and probably even lower, due to hydrolysis of dissolved aluminum ions into the unbuffered injected solution. Since the solubility of the oxide film is increased at the lower pH, partial dissolution of the porous layer may have occurred, by which I_p and the current spectral density would have increased. Injection also caused the mean current to increase for a time (on average by 40%), which would also be expected from oxide dissolution in the barrier layer or porous layer. The explanation that the enhancement of current noise is due to acidification is consistent with the observation that the low-frequency noise was not affected by injection of borate buffer itself.

Besides partial film dissolution, other explanations for these low-frequency noise features might be considered. For example, they may be related to some interaction of chloride ions with the film other than the formation of metastable pits. However, other investigations of current noise on aluminum in chloride solutions have not reported similar features.[8,9] In the present work, current bursts suggesting metastable pitting were also found after NaCl injection, but only at potentials −0.64 V vs. SCE or higher.[24] Another possibility is suggested by the work of Alwitt[34] who found that removal of borate ions from solution produced significant decreases in the resistance of the barrier layers of pseudoboehmite films on aluminum.

Conclusions

Electrochemical current noise measurements were carried out on aluminum disk microelectrodes with diameters from 25 to 508 μm. The spectral density of the current noise, S_I, in the frequency range 0.05-50 Hz was determined from current time series measured in pH 8.8 borate buffer solutions at constant potential from −1.0 to −0.7 V vs. SCE. The noise spectra had a characteristic two-plateau structure consisting of a low frequency plateau, a decay at intermediate frequency, and a high frequency plateau. The high breakpoint frequency (minimum frequency of the high frequency plateau) was identified as the characteristic resistive-capacitive frequency of the oxide film. The spectral density was potential-independent and increased uniformly with electrode area. Injection of 1 M NaCl (pH 6.1) near the electrode caused the appearance of low frequency noise features in the current time series.

A mathematical model for the current noise was formulated whose frequency and area dependences were consistent with those of the experimental spectra. The model viewed the surface film to consist of an inner solid, resistive barrier layer and an outer layer containing cracks or pores whose widths were subject to fluctuations. These fluctuations could be due to processes such as precipitation and dissolution or intermittent mechanical cracking in the oxide film. The resulting variations of the oxide film/solution interfacial area caused the potential drop across the barrier layer to fluctuate, which produced the current noise. The noise could be characterized in electrical terms as a voltage noise in series with the barrier-layer impedance. This series relationship was indicated by the identification of the high breakpoint frequency with the RC relaxation of the barrier layer. The proportionality of the current spectral density to area indicated the presence of discrete noise sources distributed approximately evenly over the electrode surface. Thus, the results suggested that the oxide layer contained separated microscopic current paths whose conductances were subject to fluctuations. However, the significance of these paths as either pores or flaws was not determined.

Acknowledgments

Support for this work was provided by the National Science Foundation under grants DMR-9006895 and DMR-9307308.

Iowa State University assisted in meeting the publication costs of this article.

List of Symbols

A	electrode area, cm^2
A_p	cross-sectional area of a pore in the porous layer, cm^2
a	microelectrode radius, cm
B	field coefficient in barrier-layer conduction rate expression, cm/V
b_c	kinetic parameter in metal ion dissolution reaction, V^{-1}
C_2	capacitance of barrier layer, F/cm^2
C_{Al}	concentration of aluminate ions at electrode surface, mol/cm^3
C_p	capacitance of oxide/solution interface, F/cm^2
D_{Al}	diffusivity of aluminate ions, cm^2/s
f	frequency, Hz
f_1, f_2, f_3	characteristic frequencies ($\omega_i/2\pi$, Hz)
g_2	conductance of barrier layer, $(\Omega\ cm^2)^{-1}$
g_3	average conductance of oxide/solution interface, $(\Omega\ cm^2)^{-1}$
g_p	local conductance of oxide/solution interface, $(\Omega\ cm^2)^{-1}$
H	random variable source term generating porosity fluctuations in porous layer, s^{-1}
I	current, A
i_{ao}	pre-exponential current density in barrier-layer conduction equation, A/cm^2
i_{co}	exchange current density for metal ion dissolution, A/cm^2
k	Boltzmann's constant, 1.3807×10^{-23} J/K
k_1, k_2	rate constants for opening and closing of pores, $cm^3/mol\ s$
N_{Al}	diffusion flux of aluminate ions, $mol/cm^2\ s$
N_o	number of open pores
N_t	number of total pores (open and closed)
n_t	number of channels in porous layer per unit electrode area, cm^{-2}
p	probability that a pore is open, dimensionless
S_H	spectral density of $H(t)$, s^{-1}
S_I	spectral density of the current noise, A^2/Hz
S_I^{th}	theoretical spectral density of current noise due to thermal conduction, A^2/Hz
T	absolute temperature, K
t	time, s
δ	thickness of barrier layer, cm
ϵ	porosity of porous layer, dimensionless
ϕ_2	potential drop across barrier layer, V
ϕ_3	potential drop across oxide/solution interface, V
σ_N^2	variance of number of open pores, dimensionless
τ	time constant, s
ω	angular frequency, radian/s
$\omega_1, \omega_2, \omega_3$	characteristic frequencies, radians/s

References

1. D. E. Williams, J. Stewart, and P. H. Balkwill, *Corros. Sci.*, **36,** 1213 (1994).
2. P. C. Pistorius and G. T. Burstein, *Mater. Sci. Forum*, **111-112**, 429 (1994).
3. H. Böhni, T. Suter, and A. Schreyer, *Electrochim. Acta*, **40**, 1361 (1995).
4. K. Nachstedt and K. E. Heusler, *Electrochim. Acta*, **33**, 311 (1988).
5. K. Nachstedt and K. E. Heusler, *Z. Phys. Chem. N. F.*, **160**, 131 (1988).
6. K. E. Heusler, K. Nachstedt, and H. Muscher, *Bull. Electrochem.*, **8**, 7 (1992).
7. U. Bertocci and J. Kruger, *Surf. Sci.*, **101**, 608 (1980).
8. R. Hollinger and H. Böhni, in *Computer Aided Acquisition and Analysis of Corrosion Data*, M. W. Kendig, U. Bertocci, and J. Strutt, Editors, PV 85-3, p. 200, The Electrochemical Society, Pennington, NJ (1984).

S0013-4651(98)01-075-1 CCC: $7.00

9. S. T. Pride, J. R. Scully, and J. L. Hudson, in *Electrochemical Noise Measurement for Corrosion Applications*, STP 1277, p. 307, J. R. Kearns, J. R. Scully, P. R. Roberge, D. L. Reichert, and J. L. Dawson, Editors, ASTM, West Conshohocken, PA (1996).
10. J. C. Uruchurtu and J. L. Dawson, *Corrosion*, **43**, 19 (1987).
11. G. C. Wood, W. H. Sutton, J. A. Richardson, T. N. K. Riley, and A. G. Malherbe, in *Localized Corrosion*, NACE-3, p. 526, B. F. Brown, J. Kruger, and R. W. Staehle, Editors, NACE, Houston, TX (1974).
12. J. R. Galvele, S. M. de De Micheli, I. L. Muller, S. B. de Wexler, and I. L. Alanis, in *Localized Corrosion*, NACE-3, p. 526, B. F. Brown, J. Kruger, and R. W. Staehle, Editors, NACE, Houston, TX (1974).
13. R. Krishnakumar and Z. Szklarska-Smialowska, *Mater. Sci. Forum*, **111-112**, 565 (1994).
14. K. Shimizu, R. C. Furneaux, G. E. Thompson, G. C. Wood, A. Gotoh, and K. Kobayashi, *Oxid. Metals*, **35**, 5/6 (1991).
15. G. M. Brown, K. Shimizu, K. Kobayashi, G. E. Thompson, and G. C. Wood, *Corros. Sci.*, **34**, 2099 (1993).
16. G. Blanc, C. Gabrielli, M. Ksouri, and R. Wiart, *Electrochim. Acta*, **23**, 337 (1978).
17. L. J. DeFelice, *Introduction to Membrane Noise*, Plenum Press, New York (1981).
18. A. van der Ziel, *Noise in Solid State Devices and Circuits*, Wiley, New York (1986).
19. G. Barker, *J. Electroanal. Chem.*, **21**, 127 (1969).
20. V. A. Tygai, *Electrochim. Acta*, **16,** 1647 (1971).
21. G. Blanc, I. Epelboin, C. Gabrielli, and M. Keddam, *J. Electroanal. Chem.*, **75**, 97 (1977).
22. C. Gabrielli, F. Huet, and M. Keddam, *Electrochim. Acta*, **31**, 1025 (1986).
23. J. O. Howell, W. G. Kuhr, R. E. Ensman, and R. M. Wightman, *J. Electroanal. Chem.*, **209**, 77 (1986).
24. J. W. Isaac, M.S. Thesis, Iowa State University, Ames, IA (1995).
25. W. Wilhelmsen and T. Hurlen, *Electrochim. Acta*, **32**, 95 (1987).
26. K. E. Heusler and W. Allgaier, *Werkst. Korros.*, **22**, 297 (1971).
27. R. S. Alwitt, in *Oxides and Oxide Films*, J. W. Diggle and A. K. Vijh, Editors, Vol. 4, p. 192, Marcel Dekker, New York (1976).
28. H. Kaesche, in *Passivity of Metals*, R. P. Frankenthal and J. Kruger, Editors, p. 939, The Electrochemical Society, Princeton, NJ (1978).
29. T. Våland and K. E. Heusler, *J. Electroanal. Chem.*, **149**, 71 (1983).
30. K. J. Vetter and F. Gorn, *Electrochim. Acta*, **18**, 321 (1973).
31. L. Young, *Anodic Oxide Films*, Academic Press, London (1961).
32. J. Bessone, C. Mayer, K. Jüttner, and W. J. Lorenz, *Electrochim. Acta*, **28**, 171 (1983).
33. H. J. W. Lenderink, M. V. D. Linden, and J. H. W. De Witt, *Electrochim. Acta*, **14**, 1989 (1993).
34. R. S. Alwitt, *J. Electrochem. Soc.*, **118**, 1734 (1971).